Antarctic Science 26(6), 636–645 (2014) doi:10.1017/S0954102014000364

Recent variations in the terminus position, ice velocity and surface elevation of Langhovde Glacier, East Antarctica

TAKEHIRO FUKUDA[1,2], SHIN SUGIYAMA[1]*, TAKANOBU SAWAGAKI[3] and KAZUKI NAKAMURA[4]

[1]*Institute of Low Temperature Science, Hokkaido University, Sapporo 060-0819, Japan*
[2]*Graduate School of Environmental Science, Hokkaido University, Sapporo 060-0810, Japan*
[3]*Faculty of Environmental Earth Science, Hokkaido University, Sapporo 060-0810, Japan*
[4]*College of Engineering, Nihon University, Koriyama 963-1165, Japan*
**corresponding author: sugishin@lowtem.hokudai.ac.jp*

Abstract: To improve the understanding of the mechanism driving recent changes in outlet glaciers in East Antarctica, we measured changes in the terminus position, ice flow velocity and surface elevation of the Langhovde Glacier located on the Sôya Coast. From satellite images from 2000–12 and field measurements taken in 2012 the glacier terminus position and flow velocity showed little change between 2003 and 2007. After this quiescent period, the glacier progressively advanced by 380 m and the flow velocity increased near the calving front by 10 m a^{-1} from 2007–10. No significant change was observed in surface elevation during the study period. The changes in the terminus position and flow velocity imply a reduction in the calving rate from 93 m a^{-1} (2003–07) to 16 m a^{-1} (2007–10). This suggests that calving was inhibited by stable sea ice conditions in the ocean. Theses results indicate that the Langhovde Glacier was in a relatively stable condition during the study period, and its terminus position was controlled by the rate of calving under the influence of sea ice conditions.

Received 16 September 2013, accepted 1 May 2014

Key words: calving, ice shelf, outlet glacier, satellite image, sea ice

Introduction

Recent satellite observations have shown rapid changes of the Antarctic ice sheet along coastal margins. Large ice shelves are rapidly retreating (Fox & Vaughan 2005, MacGregor *et al.* 2012), fast flowing outlet glaciers and ice streams are both showing increasing flow velocity (Joughin *et al.* 2003, Lee *et al.* 2012) and ice is thinning on the accelerating glaciers (Shepherd *et al.* 2001, Scott *et al.* 2009, Wingham *et al.* 2009). Acceleration and thinning of outlet glaciers are often associated with disintegration of ice shelves in front of the glaciers (Rignot *et al.* 2004, Scambos *et al.* 2004, Joughin & Alley 2011). One possibility is that basal melting of ice shelves is increasing because of warming ocean water (Pritchard *et al.* 2012), resulting in ice shelf disintegration and a consequent increase in ice velocity. Such acceleration triggers thinning of outlet glaciers because an increasing amount of ice is discharged into the ocean.

Such dynamically driven ice mass loss in outlet glaciers has been reported particularly in West Antarctica. As a consequence, mass balance of the West Antarctic Ice Sheet was -102 ± 18 Gt a^{-1} between 2005–10, showing a more negative mass balance in recent years (Shepherd *et al.* 2012 and references therein). On the other hand, the East Antarctic Ice Sheet showed a positive mass balance of $+58 \pm 31$ Gt a^{-1} during the same period (Shepherd *et al.* 2012). Monitoring fast flowing glaciers is a crucial aspect of improving our understanding of the contrasting mass balance trends in West and East Antarctica.

Despite the multitude of studies based on large-scale observations from satellites, there is a dearth of direct evidence of glacier change collected in the field. Field data is needed to calibrate satellite observations, as well as to examine mechanisms driving the observed changes. Most of the recent detailed research has focused on outlet glaciers in West Antarctica (Scambos *et al.* 2004, Shuman *et al.* 2011, Berthier *et al.* 2012). There are a number of outlet glaciers along the coast of East Antarctica, but only a few of them have been studied thus far (Stearns *et al.* 2008, Yu *et al.* 2010, Callens *et al.* 2013, Miles *et al.* 2013). Further studies are required to understand ongoing changes in East Antarctica and shed light on mechanisms driving the mass balance trend in the Antarctic ice sheet.

The focus of this study was Langhovde Glacier, an outlet glacier flowing into an ice shelf on the Sôya Coast in East Antarctica. Data presented in this paper, mostly from the floating part of the glacier, combine satellite-based observations and field measurements to quantify changes in the terminus position, flow velocity and surface elevation from 2000–12.

Study site

Langhovde Glacier (69°11'S, 39°32'E) (Fig. 1a) is located at the coast of Lützow-Holm Bay on the Sôya Coast

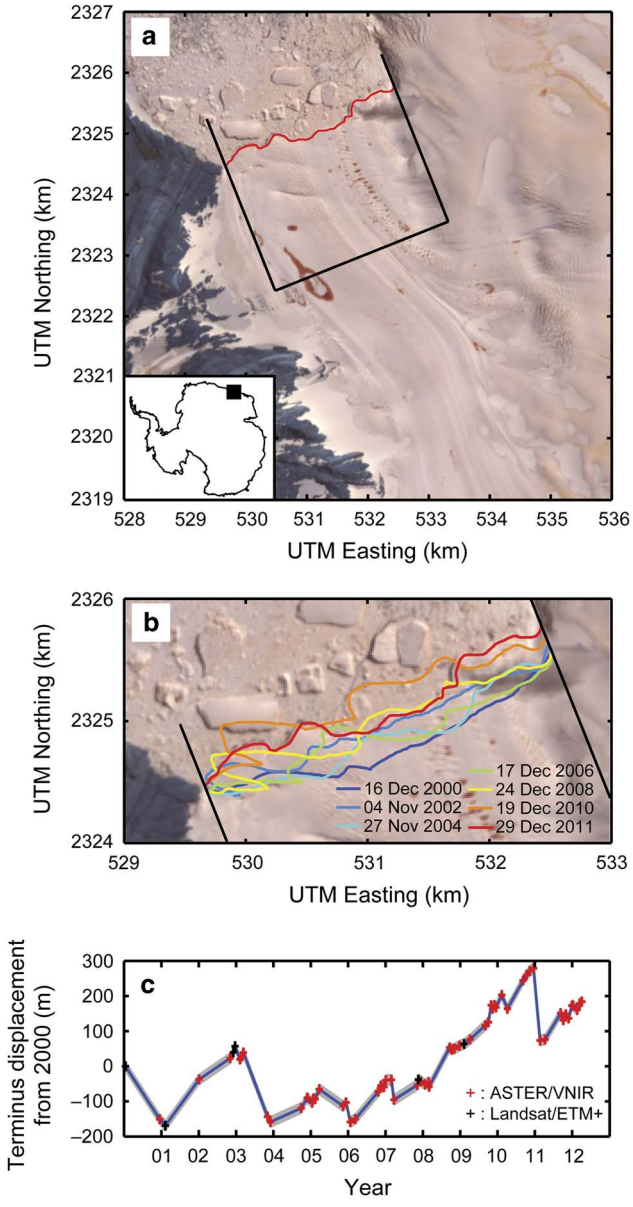

Fig. 1a. An ASTER-VNIR image from 29 December 2011, showing the Langhovde Glacier, with the inset showing the study area within Antarctica. The glacier frontal margin is indicated by the red line. Changes in the area within the frontal margin and the black lines are measured to compute mean terminus displacement. **b.** The glacier frontal margins during 2000–11. **c.** Terminus displacement relative to the position on 15 January 2000. The data obtained from ASTER-VNIR and Landsat7/ETM+ are indicated by red and black crosses, respectively. Measurement error is indicated by the width of the grey line connecting the data.

c. 20 km south of Syowa Station, a Japanese Antarctic Research Expedition (JARE) base. The Sôya coast region has been intensively studied by JARE for the past several decades, but glaciological studies in this coastal region are limited (Nakawo *et al.* 1978, Iizuka *et al.* 2001, Nakamura *et al.* 2007). This study focused on Langhovde as the glacier is within the reach of helicopter operation from Syowa Station and the ice surface is relatively safe for fieldwork. Although the glacier is relatively small, it has the typical structure of an Antarctic outlet glacier.

Langhovde Glacier is 3 km wide at the calving front and the fast flowing part is *c*. 10 km long (Fig. 1a). The ice surface is flat in the lower few kilometres, suggesting the formation of a floating tongue. The glacier is bound by relatively slowly moving ice to the east and bedrock to the west. The glacier flows faster than the surrounding ice and discharges ice into the ocean by calving. The glacier front is in contact with Antarctic Surface Water (Whitworth *et al.* 1998), which fills the upper layer in Lützow-Holm Bay (Ohshima *et al.* 1996). According to previous studies, Langhovde Glacier has been relatively stable over a period of decades to millennia. Miura *et al.* (1998) dated fossil shells from beach deposits at *c*. 3 km from the current glacier front, and concluded that this location had been ice free over the last 5000 years. Komazawa (2014) used aerial photographs and satellite images to analyse the frontal variations from 1975–2007 and found only 400 m retreat during the period. Presumably the ice front position is controlled by the valley width, which spreads offshore from the current glacier front (Fig. 1a).

Methods

Satellite image analysis was performed for the glacier terminus position, flow velocity and surface elevation over the period between 2000–12. The lower 5 km of the glacier was analysed in 6 km × 6 km images cropped from several different types of satellite visible images. Field measurements of flow velocity and surface elevation were also made in the lower 3.5 km of the glacier from January to February 2012 as a part of the 53rd JARE programme.

Terminus position

Panchromatic band 8 images obtained by the Enhanced Thematic Mapper Plus (ETM+) mounted on Landsat 7, and visible and near-infrared (VNIR) band 3N images obtained by the Advanced Spaceborne Thermal Emission and Reflection (ASTER) radiometer, were orthorectified and supplied by the US Geological Survey and by the Earth Remote Sensing Data Analysis Center in Japan, respectively. The spatial resolution of the images is 15 m. Specific dates and other satellite image information used are summarized in Table I.

The glacier frontal margin was manually delineated on each image using GIS software (ArcGIS10, ESRI).

https://doi.org/10.1017/S0954102014000364 Published online by Cambridge University Press

Table I. ETM+ and ASTER images used to measure terminus position.

Period	Acquisition date	
	ETM+ (6 images)	ASTER (57 images)
1999–00	15 Jan 2000	
2000–01	9 Feb 2001	16 Dec 2000
2001–02		4 Jan 2002
2002–03	6 Dec, 22 Dec 2002	4 Nov 2002, 8 Feb, 26 Feb, 14 Mar 2003
2003–04		5 Nov, 2 Dec 2003
2004–05		29 Sep, 27 Nov 2004, 14 Jan, 26 Jan, 13 Feb, 24 Mar 2005
2005–06		14 Nov, 12 Dec 2005, 22 Jan, 11 Mar 2006
2006–07		23 Oct, 17 Nov, 17 Dec 2006, 4 Jan, 28 Feb, 25 Mar 2007
2007–08	18 Nov 2007	9 Nov, 13 Dec 2007, 23 Jan, 29 Feb, 2 Mar 2008
2008–09	8 Feb 2009	19 Sep, 10 Oct, 4 Nov, 24 Dec 2008, 6 Apr 2009
2009–10		2 Sep, 4 Oct, 31 Oct, 14 Nov, 2 Dec, 16 Dec 2009, 11 Feb, 7 Apr 2010
2010–11		7 Sep, 11 Oct, 12 Nov, 19 Dec 2010, 21 Feb, 10 Apr 2011
2011–12		10 Sep, 5 Oct, 30 Oct, 27 Nov, 29 Dec 2011, 7 Jan, 19 Feb, 13 Mar, 5 Apr 2012

By comparing the time series of satellite images, changes in the glacier surface area near the calving front were measured for each time interval (Fig. 1b). This aerial change was divided by the width of the calving front to obtain the mean displacement of the glacier front (Moon & Joughin 2008). Potential errors in the measurement include misalignment of satellite images and uncertainties in the manual delineation process. Five ground control points (GCPs) were used for each image pair to minimize misalignment. Consequently, the root mean square error of GCPs was 23 m. Uncertainties in the delineation were evaluated by repeating the procedure for one of the images. The standard deviation of the 20 measurements was 2.4 m. Thus, the total error in this analysis is assumed to be 25 m.

Flow velocity

Flow velocities from 2003–12 were measured by using a feature tracking analysis of ASTER images. The same image type was used as for the terminus position measurements (VNIR, band 3N), orthorectified listed in Table II. Displacements of ice surface features were measured using COSI-Corr, software provided by California Institute of Technology (a plug-in for a remote-sensing platform ENVI (ESRI), a geospatial imagery analysis and processing application). COSI-Corr calculates horizontal displacements of surface features by computing spatial correlations between a multi-temporal image pair with sub-pixel resolution (Leprince *et al.* 2007, Scherler *et al.* 2008, Herman *et al.* 2011). Using 40 image pairs with intervals of *c.* 1 year between 2003–12 cross-correlation coefficients were computed with a reference window defined on the first image over a search window defined on the second image. The size of the reference window was 32×32–16×16 pixels depending on the magnitude of the displacement.

This provided horizontal components of the surface displacement and the signal-to-noise ratio (SNR) for an area of 6 km × 6 km near the glacier terminus with a spatial resolution of 15 m. The ASTER images were

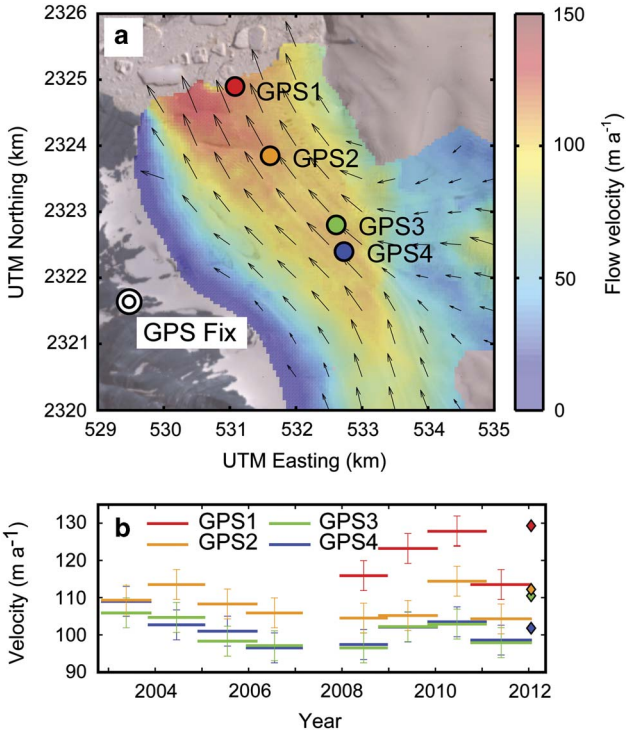

Fig. 2a. Velocity vectors and horizontal velocity (colour scale) between 5 January 2011 and 24 January 2012 obtained by feature tracking analysis. Locations of ice velocity measurement sites (GPS1–4) and GPS reference station (GPS Fix) are indicated. The background is an ASTER image from 24 January 2012. **b.** Ice flow velocities at GPS1–4 from 2003–12. The widths of the markers indicate the period of COSI-Corr analysis. Data obtained by field GPS measurements are indicated with diamonds.

https://doi.org/10.1017/S0954102014000364 Published online by Cambridge University Press

Table II. ASTER image pairs used for the velocity measurements.

Period	Acquisition date		Interval
	Pre-image	Post-image	(days)
2002–03 to 2003–04	04 Nov 2002	05 Nov 2003	366
	04 Nov 2002	02 Dec 2003	393
	14 Mar 2003	05 Nov 2003	236
	14 Mar 2003	02 Dec 2003	263
2003–04 to 2004–05	05 Nov 2003	27 Nov 2004	388
	05 Nov 2003	26 Jan 2005	448
	02 Dec 2003	27 Nov 2004	361
	02 Dec 2003	26 Jan 2005	421
2004–05 to 2005–06	27 Nov 2004	23 Dec 2005	391
	27 Nov 2004	11 Mar 2006	469
	26 Jan 2005	23 Dec 2005	331
	26 Jan 2005	11 Mar 2006	409
2005–06 to 2006–07	12 Dec 2005	17 Nov 2006	340
	12 Dec 2005	28 Feb 2007	443
	11 Mar 2006	17 Nov 2006	251
	11 Mar 2006	28 Feb 2007	354
2006–07 to 2007–08	28 Feb 2007	23 Jan 2008	329
	28 Feb 2007	29 Feb 2008	366
2007–08 to 2008–09	13 Dec 2007	10 Oct 2008	302
	23 Jan 2008	24 Dec 2008	336
2008–09 to 2009–10	10 Oct 2008	31 Oct 2009	386
	10 Oct 2008	16 Dec 2009	432
	24 Dec 2008	31 Oct 2009	311
	24 Dec 2008	19 Jan 2010	391
2009–10 to 2010–11	31 Oct 2009	02 Oct 2010	336
	31 Oct 2009	19 Dec 2010	414
	31 Oct 2009	05 Feb 2011	462
	16 Dec 2009	02 Oct 2010	290
	16 Dec 2009	19 Dec 2010	368
	16 Dec 2009	05 Feb 2011	416
	19 Jan 2010	05 Feb 2011	382
2010–11 to 2011–12	02 Oct 2010	05 Oct 2011	368
	02 Oct 2010	27 Nov 2011	421
	02 Oct 2010	25 Jan 2012	480
	19 Dec 2010	29 Dec 2011	375
	19 Dec 2010	07 Jan 2012	384
	19 Dec 2010	25 Jan 2012	402
	05 Feb 2011	29 Dec 2011	327
	05 Feb 2011	07 Jan 2012	336
	05 Feb 2011	25 Jan 2012	354

orthorectified based on the digital elevation models (DEMs) supplied with the images, and the DEMs have relatively greater errors over a snow surface, low-contrast area and steep slopes. These errors in the DEM result in miscorrelations in the cross-correlation analysis. To minimize errors due to miscorrelations, data with a SNR > 0.90 were removed and a median filter was applied to the displacement field. Flow velocities at the GPS measurement sites were computed by interpolating the 2D velocity fields.

The accuracy of the velocity measurements were evaluated by computing the displacement between images separated by a short period, a so-called null test (Berthier *et al.* 2012). By processing two image pairs with an interval of 2 days (10–12 October 2008 and 14–16 November 2009), the standard error arising from the cross-correlation analysis was determined to be 4.0 m. The separation of image pairs used for the velocity measurements was 0.65–1.32 years. Thus, the uncertainty in the velocity was 3.0–6.2 m a^{-1}.

Table III. ALOS/PRISM stereo image pairs used for the DEM generation. B, N and F denote back, nadir and forward images.

Acquisition date		Scene ID
16 Nov 2006	B, N	ALPSMB043205070
		ALPSMN043205015
29 Nov 2007	B, N, F	ALPSMB096885070
		ALPSMN096885015
		ALPSMF096884960
10 Nov 2010	B, N	ALPSMB255445070
		ALPSMN255445015

Ice surface velocity was measured in the field from 2–29 January 2012 by surveying aluminium poles installed on the glacier 0.4–3.3 km from the terminus. To survey the positions of these poles, two types of dual-frequency GPS receivers were used: GEM-1 (GNSS Technologies) and System1200 (Leica Geosystems). The GPS antennae were mounted on the top of the survey poles, which were drilled > 1.0 m deep into the ice (Fig. 2a, GPS1–4). Another GPS antenna and receiver (GEM-1) was placed on bedrock to the west of the glacier (Fig. 2a, GPS Fix) to serve as a reference station. The distance from the reference station to the survey poles was 3.1–3.6 km. The GPS data were post-processed to compute the 3D coordinates of the poles with a static positioning technique. The measurements were repeated on 5 and 29 January 2012 to measure the displacement during this period. The GPS positioning accuracy expected for the baseline length was 5 mm. An error caused by the tilt of the survey poles was less than a few centimetres. Thus, the measurement error was < 0.05 m, which is equivalent to a velocity error of < 1.0 m a^{-1}.

Surface elevation

Glacier surface elevation was measured by stereographic analysis of satellite images captured by the Panchromatic Remote-sensing Instrument for Stereo Mapping (PRISM) on the Advanced Land Observing Satellite (ALOS). The images used for this study were taken on 16 November 2006, 29 November 2007 and 10 November 2010 (Table III). The ALOS/PRISM images were radiometrically and geometrically corrected (Level 1B2) and accompanied with a rational polynomial coefficient file, which described the parameters needed for converting the image pixels to geographical coordinates. The resolution of the image was 2.5 m.

The stereographic analysis was performed with a digital photogrammetry system, consisting of a stereo mirror 3D

https://doi.org/10.1017/S0954102014000364 Published online by Cambridge University Press

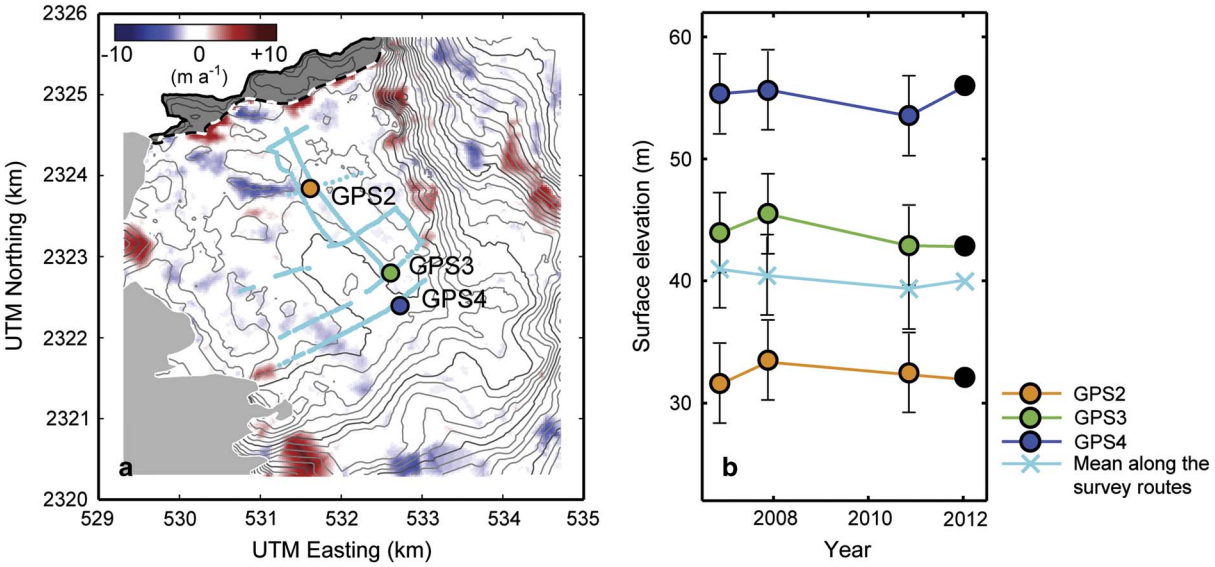

Fig. 3a. Surface elevation change from 10 November 2006–17 November 2010. Elevation change is illustrated only on the glacier surface, and bedrock is indicated by grey. The cyan dots indicate the measurement points of GPS survey. The contour lines show surface elevation in 2010 with 10 m intervals. Dashed and solid lines indicate the terminus positions on 10 November 2006 and 17 November 2010, respectively. **b.** Surface elevation at GPS2–4 and mean elevation along the GPS survey routes from 2006–12. Data obtained by DEMs and field GPS surveys are indicated by colour and black symbols, respectively.

monitor (SD2020, Planar Systems), 3D mouse (TopoMouse, Leica Geosystems) and Leica Photogrammetric Suite 2011 (LPS) mounted on an ERDAS IMAGE 2011 platform (Intergraph Corporation). A stereographic image pair was co-registered using one or more GCPs obtained from a 1:25 000 topographic map for JARE (Geographical Survey Institute, http://geogisopen.nipr.ac.jp/gisopen/). The LPS automatically generates a polygonal surface from a stereo image pair, but this surface has substantial errors, particularly in low contrast regions such as snow surfaces, shadows and steep slopes (Toutin 2002). To improve accuracy, the elevation was manually corrected on the stereographic view using the 3D monitor and the 3D mouse. After this manual correction, a 10 m mesh DEM was generated by interpolating the polygonal surface (Lamsal *et al.* 2011). To estimate errors in the generated DEMs, the three DEMs were compared over a bedrock area, where vertical displacement was assumed to be zero. The mean standard deviation evaluated over a 1 km^2 bedrock surface was 3.2 m, similar to that reported in a previous study by Lamsal *et al.* (2011).

Glacier surface elevation was measured in the field on 24 and 25 January 2012, using a kinematic GPS positioning technique. Ice was exposed on the glacier surface in the region of study during the survey period. In this survey, the same reference station was employed as for the velocity measurement. The antenna of another GPS (System1200) was mounted on top of a 2 m long survey pole to record GPS signals every second as a rover station. The survey pole was held vertical to the ice surface by hand to make a measurement for 15 seconds. We surveyed 382 locations over the region, approximately every 100 m along seven survey routes (Fig. 3a). The accuracy of the kinematic GPS positioning is *c.* 10 mm. By taking other error sources (e.g. tilt of the survey pole, surface micro roughness), the measurement error in the vertical direction was assumed to be < 0.1 m. Since our study area is located mostly on floating ice, vertical ice motion due to tides has to be taken into account. According to our GPS measurements performed in the field (Sugiyama *et al.* 2014), tidal motion is up to 1.5 m at GPS1 and 0.5 m at GPS2. This uncertainty progressively decreases up-glacier and is negligible at GPS3 and GPS4.

Results

Terminus position

The glacier terminus advanced by 180 m from 2000–12 after variations within a distance of 450 m (Fig. 1b & c). At the beginning of this period, the glacier showed a sudden retreat of 170 m from 2000–01 and 180 m in 2003. These sudden retreats coincided with large calving events which occurred after the summers of 2000–01 and 2002–03. The exact timings of the events are not known as images are not available for the winter. After these two events, the terminus advanced by 380 m from January 2007–January 2010. During this period, large icebergs were not observed in front of the glacier. Another calving

https://doi.org/10.1017/S0954102014000364 Published online by Cambridge University Press

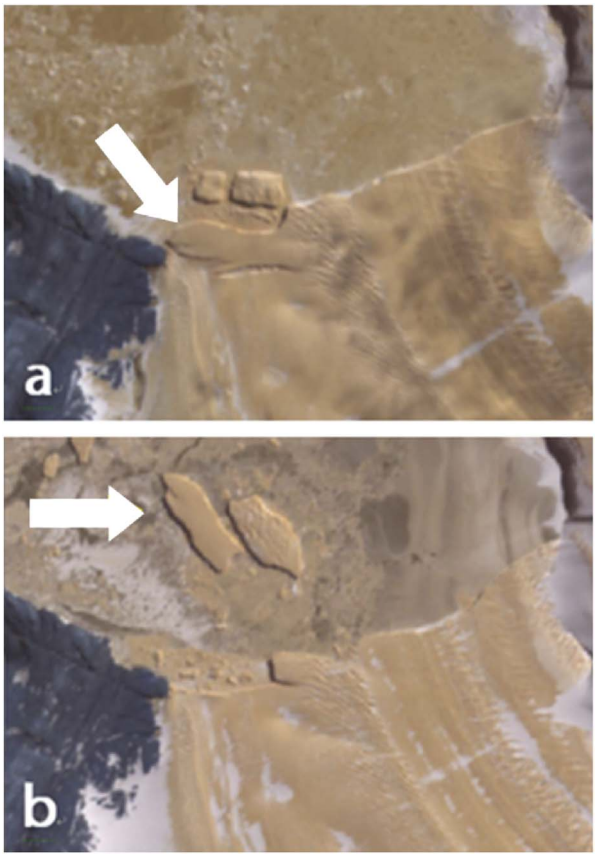

Fig. 4. ASTER-VNIR images captured on **a.** 11 November 2002 and **b.** 2 December 2003. Arrows indicate the same ice block before and after calving.

event occurred in January 2011, resulting in a 200 m retreat. According to the images over the study period, relatively large icebergs (400–500 m long) were detached from the western half of the calving front (Fig. 4), whereas smaller and more frequent calving events were observed in the eastern half. The mean rate of glacier advance over the period from 2000–12 was 15 m a^{-1}.

Flow velocity

A 2D flow velocity field between 5 January 2011 and 25 January 2012 is shown in Fig. 2a. The maximum velocity is 128 m a^{-1} observed at the glacier centre near the terminus. The velocity field showed a glacier flowing into the terminus region from the south and east. These two tributaries were merged in our study region. It showed that the velocity along the central flow-line was > 100 m a^{-1}.

Velocity was interpolated at the GPS measurement sites to investigate temporal variations from 2003–12 (Fig. 2b). The data show complex velocity variations over the study period, which were significantly greater than the measurement errors. At GPS2, velocity decreased from 2003–08 by 9.0 m a^{-1}, followed by an increase of 9.9 m a^{-1} in the period from 2008–10. The velocity fell in 2011, but the velocity obtained by the field GPS measurement in January 2012 was greater than the long-term mean velocity from October 2010–February 2012. It should be noted that the field measurement represents the summer velocity, whereas the other satellite-derived data are mean velocity over *c.* 1 year. These changes were also observed at two other GPS sites. While the timings of the velocity changes were similar at the three locations, the acceleration in 2008–09 was initiated earlier near the terminus (GPS1) than in the upper reaches (GPS2–4).

Surface elevation

Changes in surface elevation were calculated by differentiation of DEMs. Glacier surface elevation showed little variation over the study period. The rate of surface elevation change in the study region was from +4.9–-8.8 m a^{-1} between 2006–10 (Fig. 3a). There were several regions where elevation change was greater than the vertical error of the DEMs (3.2 m). However, these changes were due to the advection of surface topographical features (e.g. crevasses, bumps and depressions) or snow deposition on a relatively steep surface. These surface features were observable on the satellite images, and also confirmed by *in situ* observations during the field campaign in 2011. There was no general trend in elevation change at the three GPS sites or along the kinematic GPS survey routes (Fig. 3b). The mean elevation change over the 382 survey locations along the survey routes was only -0.3 m a^{-1} between 2006–12. The magnitudes of the elevation changes

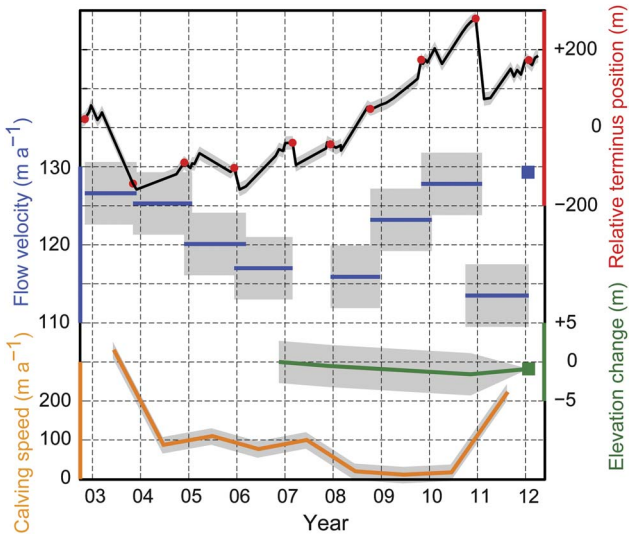

Fig. 5. Terminus displacement relative to 15 January 2000 (black line with red dots), flow velocity at GPS1 (blue line), mean surface elevation change along the GPS survey routes (green line) and calculated calving speed (yellow line) of Langhovde Glacier from 2003–12. Error ranges are indicated by the grey bands.

https://doi.org/10.1017/S0954102014000364 Published online by Cambridge University Press

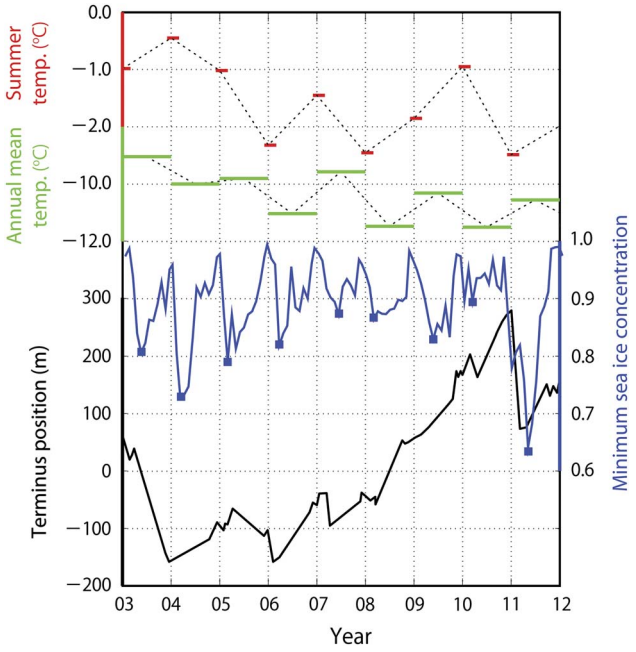

Fig. 6. Variations in the terminus position (black), air temperatures at Syowa Station (green: annual mean, red: summer mean), and minimum sea ice concentration in Lützow-Holm Bay (blue).

were smaller than the DEM error. Thus, the DEM analyses and GPS field survey show no significant elevation change in the survey area from 2006–12.

Discussion

The changes in the terminus position, flow velocity and surface elevation between 2003–12 are compared in Fig. 5. In addition to this observational data, the calving rate was calculated by subtracting the rate of the terminus displacement from the velocity near the glacier front. Two relatively large calving events occurred in 2003 and 2011, resulting in significant retreats of the terminus position. This observation indicates that the terminus position of Langhovde Glacier is primarily controlled by sporadic large calving events, rather than changes in ice velocity. The calving rate was relatively constant at 77–110 m a^{-1} (a mean of 93 m a^{-1}) between 2004–07, and was reduced to 11–19 m a^{-1} (a mean of 16 m a^{-1}) from 2008–10. Velocity increase was also observed from 2009–10. Thus, the progressive advance from 2007–11 was driven by a combination of ice velocity increase and calving rate reduction.

The foregoing discussion demonstrates that the calving rate plays an important role in the frontal variations of Langhovde Glacier. To investigate the control of the calving rate variations, air temperature measured at Syowa Station was compared with our data (Fig. 6).

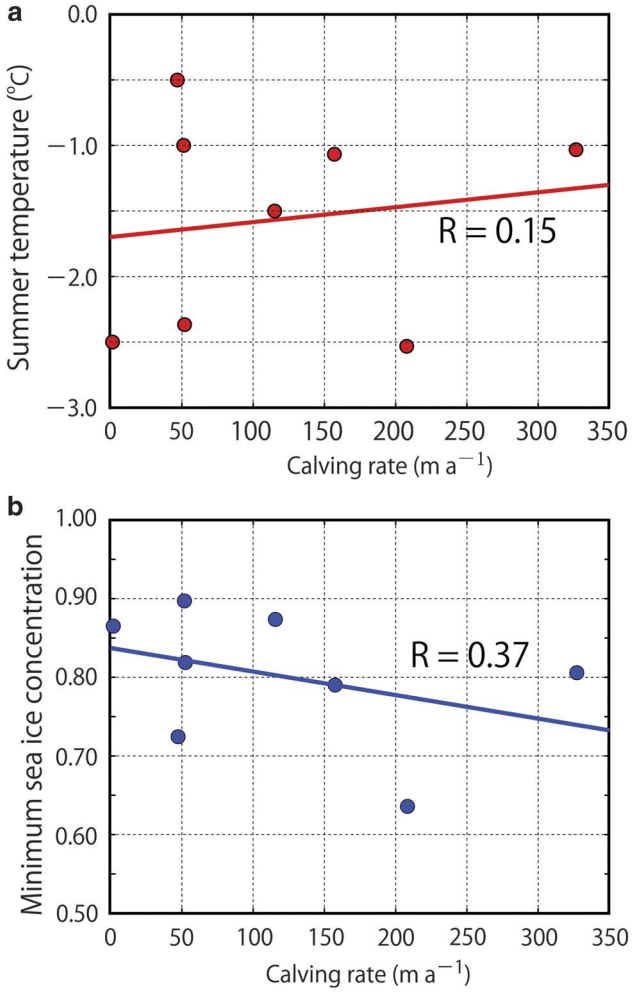

Fig. 7. Scatter plots of **a.** the calving rate of Langhovde Glacier and summer mean air temperature at Syowa Station (correlation coefficient $r = 0.15$, $P = 0.63$) and **b.** the calving rate and minimum sea ice concentration in Lützow-Holm Bay ($r = 0.37$, $P = 0.21$).

The calving rate dropped in 2008, but annual mean air temperature showed no marked change. The temperature trend at Syowa Station from 2000–12 was -0.078°C a^{-1}. Similarly, summer mean temperature (the average of monthly mean air temperatures in December, January and February) showed a very slightly negative trend (-0.020°C a^{-1}). The correlation coefficient between the calving rate and the summer mean temperature was 0.15 ($P = 0.63$) (Fig. 7a). Thus, it seems unlikely that the calving rate of Langhovde Glacier is controlled by air temperature in the region.

Sea ice conditions in the Lützow-Holm Bay, where Langhovde Glacier terminates, are possible drivers of the calving rate change. Ushio *et al.* (2006) reported relatively unstable (thin and low concentration) sea ice cover from the late 1990s to 2006. After this period, sea ice disintegrated and flowed out from the bay in July 2006

https://doi.org/10.1017/S0954102014000364 Published online by Cambridge University Press

(Ushio 2010). After this opening of the bay, heavy snow accumulation produced thick superimposed ice on newly formed sea ice, with the sea ice becoming thicker, producing a stable condition (Ushio 2012). Recent increase in snowfall in East Antarctica, especially in Dronning Maud Land and Enderby Land, has also been reported (Boening *et al.* 2012). Thus, we hypothesize that this sea ice stabilized the glacier terminus, and inhibited the calving processes (Reeh *et al.* 2001).

To investigate the influence of sea ice on the calving rate of Langhovde Glacier, the sea ice concentration in the vicinity of the glacier terminus using satellite data from 2000–12 was analysed. The Climate Data Record of Passive Microwave Sea Ice Concentration provided by that National Oceanic and Atmospheric Administration's (NOAA) National Snow and Ice Data Center (http://nsidc.org/data/seaice/pm.html) was used. Monthly mean sea ice concentration at 14 measurement sites in Lützow-Holm Bay were analysed. The sea ice concentration generally increased from 2004–10 and suddenly dropped in 2011 (Fig. 6). The large calving events in 2004 and 2011 occurred during a period of low sea ice concentration. Since sea ice weakening during the summer period is most relevant to calving, the analysis focused on annual variations in the minimum sea ice concentration most frequently recorded between January and March. The correlation coefficient between the minimum sea ice concentration and the calving rate from 2003–12 was 0.37 ($P = 0.21$) (Fig. 7b). This calculation shows a relatively weak but significant positive correlation between the sea ice concentration and calving, implying that summer sea ice conditions in Lützow-Holm Bay play a crucial role in the calving and frontal variations of Langhovde Glacier.

Recent variations in outlet glaciers in East Antarctica are reported further east from the study site. Miles *et al.* (2013) studied frontal variations of 175 glaciers in East Antarctica along the coast at 90°–170°E. For the period 2000–10, the mean terminus displacement rate of the glaciers studied was -17.9 m a^{-1} with a median value of 8.4 m a^{-1}. The slight advance observed in Langhovde Glacier from 2000–12 gives a rate of 15 m a^{-1}, which is similar to their median value. They argued that greater changes were observed in larger and faster flowing glaciers, which may explain the relatively stable behaviour of Langhovde Glacier. They also pointed out the importance of sea ice conditions on the variations of outlet glaciers in East Antarctica (Miles *et al.* 2013). The influence of sea ice on glacier variation has also been reported by Frezzotti & Polizzi (2002). Thus, our data provides support to these studies in East Antarctica. As seen in previous studies, outlet glaciers behave differently depending on their size, flow rate and other geometrical conditions (e.g. constraint of the terminus by fjord walls, length of floating extension). Detailed studies on each individual glacier are needed to understand the precise drivers of variations in outlet glaciers.

Conclusions

In recent years, Antarctic ice sheet margins have been rapidly changing. Notably, changes in the mass balance of ice sheet and outlet glaciers, such as large scale calving, flow acceleration and ice thinning, have been observed in West Antarctica. However, the mass balance of the East Antarctic Ice Sheet has seen different patterns. While West Antarctic outlet glaciers have reported significant change, there have been no such reports in East Antarctica. The importance of detailed research in East Antarctica is becoming increasingly apparent. To have a better understanding of the causes and mechanisms of change in outlet glaciers, we focused on the terminus changes, ice thickness and velocity variations of Langhovde Glacier in East Antarctica.

The surface elevation change from 2006–12 was within 2.7 m. This small change in elevation indicates a relatively stable condition during the study period, but the terminus position showed interesting variations within a limited distance. The terminus position showed complex variations under the influence of calving events and ice velocity changes during the period. The glacier progressively advanced by 380 m from 2007–10. Velocity gradually decreased from 2003–08, and then increased by 9.9 m a^{-1} from 2008–10. It seems that the changes in the terminus position were influenced by flow velocity because these changes occurred during the same period. However, the observed advance was not due to a flow velocity change, but influenced more by the reduction in the calving rate in 2007.

Investigating the probable causes of the large calving events, we compared the calving rate with air temperature and with the sea ice concentration in front of the glacier. There was no clear trend in the annual mean temperature record during the study period, and thus no correlation between the calving rate and the summer temperature. On the other hand, the discharge of sea ice out of Lützow-Holm Bay in the summer of 2006 was related to the increase in the calving rate. Moreover, reduction in the calving rate in 2008–11 coincided with the formation of thick sea ice caused by heavy snowfall during this period. This data suggests that the calving rate of Langhovde Glacier is affected by sea ice conditions. Thinning or thickening of sea ice in front of outlet glaciers has the potential to drive rapid advancement and retreat of glacier fronts.

Acknowledgements

This research was carried out as a part of the JARE53 programme. We thank the members of JARE53 and 52 for their help in the field. The field activity was financially

supported by the National Institute of Polar Research, and the research project was funded by JSPS KAKENHI Grant Number 23651002 (2011–14). We used ASTER data β processed by AIST GEO Grid, using ASTER data owned by METI and NASA. We thank D. White and C. Stokes for providing insightful comments, and the Scientific Editor R. Bingham for handling the paper.

Author contributions

T.F. and S.S. designed the research and wrote the manuscript. T.F., T.S. and K.N. analysed satellite images. T.F., S.S. and T.S. performed field measurements. All authors discussed the results and commented on the manuscript.

References

Berthier, E., Scambos, T.A. & Shuman, C.A. 2012. Mass loss of Larsen B tributary glaciers (Antarctic Peninsula) unabated since 2002. *Geophysical Research Letters*, **39**, 10.1029/2012GL051755.

Boening, C., Lebsock, M., Landerer, F. & Stephens, G. 2012. Snowfall-driven mass change on the East Antarctic Ice Sheet. *Geophysical Research Letters*, **39**, 10.1029/2012GL053316.

Callens, D., Matsuoka, K., Steinhage, D., Smith, B. & Pattyn, F. 2013. Transition of flow regime along a marine-terminating outlet glacier in East Antarctica. *The Cryosphere Discussion*, **7**, 4913–4936.

Fox, A.J. & Vaughan, D.G. 2005. The retreat of Jones Ice Shelf, Antarctic Peninsula. *Journal of Glaciology*, **51**, 555–560.

Frezzotti, M. & Polizzi, M. 2002. 50 years of ice-front changes between the Adélie and Banzare coasts, East Antarctica. *Annals of Glaciology*, **34**, 235–240.

Herman, F., Anderson, B. & Leprince, S. 2011. Mountain glacier velocity variation during a retreat/advance cycle quantified using sub-pixel analysis of ASTER images. *Journal of Glaciology*, **57**, 197–207.

Iizuka, Y., Satake, H., Shiraiwa, T. & Naruse, R. 2001. Formation processes of basal ice at Hamna Glacier, Sôya Coast, East Antarctica, inferred by detailed co-isotopic analyses. *Journal of Glaciology*, **47**, 223–231.

Joughin, I., Rignot, E., Rosanova, C.E., Lucchitta, B.K. & Bohlander, J. 2003. Timing of recent accelerations of Pine Island Glacier, Antarctica. *Geophysical Research Letters*, **30**, 10.1029/2003GL017609.

Joughin, I. & Alley, R.B. 2011. Stability of the West Antarctic Ice Sheet in a warming world. *Nature Geoscience*, **4**, 506–513.

Komazawa, K. 2014. *Compilation of aerial photographs and measurement of ice sheet elevation change using stereo pair images along the Sôya Coast, East Antarctica*. MSc thesis, Graduate School of Environmental Science, Hokkaido University, 102 pp [in Japanese]. [Unpublished].

Lamsal, D., Sawagaki, T. & Watanabe, T. 2011. Digital terrain modelling using Corona and ALOS PRISM data to investigate the distal part of Imja Glacier, Khumbu Himal, Nepal. *Journal of Mountain Science*, **8**, 390–402.

Lee, H., Shum, C.K., Howat, I.M., Monaghan, A., Ahn, Y., Duan, J.B., Guo, J.Y., Kuo, C.Y. & Wang, L. 2012. Continuously accelerating ice loss over Amundsen Sea catchment, West Antarctica, revealed by integrating altimetry and GRACE data. *Earth and Planetary Science Letters*, **321**, 74–80.

Leprince, S., Barbot, S., Ayoub, F. & Avouac, J.P. 2007. Automatic and precise orthorectification, coregistration, and subpixel correlation of satellite images, application to ground deformation measurements. *IEEE Transactions on Geoscience and Remote Sensing*, **45**, 1529–1558.

MacGregor, J.A., Catania, G.A., Markowski, M.S. & Andrews, A.G. 2012. Widespread rifting and retreat of ice–shelf margins in the eastern Amundsen Sea embayment between 1972 and 2011. *Journal of Glaciology*, **58**, 458–466.

Miles, B.W.J., Stokes, C.R., Vieli, A. & Cox, N.J. 2013. Rapid, climate-driven changes in outlet glaciers on the Pacific coast of East Antarctica. *Nature*, **500**, 563–566.

Miura, H., Moriwaki, K., Maemoku, H. & Hirakawa, K. 1998. Fluctuations of the East Antarctic ice-sheet margin since the last glaciation from the stratigraphy of raised beach deposits along the Sôya Coast. *Annals of Glaciology*, **27**, 297–301.

Moon, T. & Joughin, I. 2008. Changes in ice front position on Greenland's outlet glaciers from 1992 to 2007. *Journal of Geophysical Research - Earth Surface*, **113**, 10.1029/2007JF000927.

Nakamura, K., Doi, K. & Shibuya, K. 2007. Estimation of seasonal changes in the flow of Shirase Glacier using JERS-1/SAR image correlation. *Polar Science*, **1**, 73–83.

Nakawo, M., Ageta, U. & Yoshimura, A. 1978. Discharge of ice across the Sôya Coast. *Memoirs of National Institute of Polar Research - Special Issue*, **7**, 235–244.

Ohshima, K.I., Takizawa, T., Ushio, S. & Kawamura, T. 1996. Seasonal variations of the Antarctic coastal ocean in the vicinity of Lützow-Holm Bay. *Journal of Geophysical Research - Oceans*, **101**, 20 617–20 628.

Pritchard, H.D., Ligtenberg, S.R.M., Fricker, H.A., Vaughan, D.G., van den Broeke, M.R. & Padman, L. 2012. Antarctic ice-sheet loss driven by basal melting of ice shelves. *Nature*, **484**, 502–505.

Reeh, N., Thomsen, H.H., Higgins, A.K. & Weidick, A. 2001. Sea ice and the stability of north and northeast Greenland floating glaciers. *Annals of Glaciology*, **33**, 474–480.

Rignot, E., Casassa, G., Gogineni, P., Krabill, W., Rivera, A. & Thomas, R. 2004. Accelerated ice discharge from the Antarctic Peninsula following the collapse of Larsen B ice shelf. *Geophysical Research Letters*, **31**, 10.1029/2004GL020697.

Scambos, T.A., Bohlander, J.A., Shuman, C.A. & Skvarca, P. 2004. Glacier acceleration and thinning after ice shelf collapse in the Larsen B embayment, Antarctica. *Geophysical Research Letters*, **31**, 10.1029/2004GL020670.

Scherler, D., Leprince, S. & Strecker, M.R. 2008. Glacier-surface velocities in alpine terrain from optical satellite imagery: accuracy improvement and quality assessment. *Remote Sensing of Environment*, **112**, 3806–3819.

Scott, J.B.T., Gudmundsson, G.H., Smith, A.M., Bingham, R.G., Pritchard, H.D. & Vaughan, D.G. 2009. Increased rate of acceleration on Pine Island Glacier strongly coupled to changes in gravitational driving stress. *Cryosphere*, **3**, 125–131.

Shepherd, A., Wingham, D.J., Mansley, J.A.D. & Corr, H.F.J. 2001. Inland thinning of Pine Island Glacier, West Antarctica. *Science*, **291**, 862–864.

Shepherd, A., Ivins, E.R., Geruo, A. & 43 others. 2012. A reconciled estimate of ice-sheet mass balance. *Science*, **338**, 1183–1189.

Shuman, C.A., Berthier, E. & Scambos, T.A. 2011. 2001–2009 elevation and mass losses in the Larsen A and B embayments, Antarctic Peninsula. *Journal of Glaciology*, **57**, 737–754.

Stearns, L.A., Smith, B.E. & Hamilton, G.S. 2008. Increased flow speed on a large East Antarctic outlet glacier caused by subglacial floods. *Nature Geoscience*, **1**, 827–831.

Sugiyama, S., Sawagaki, T., Fukuda, T. & Aoki, S. 2014. Active water exchange and life near the grounding line of an Antarctic outlet glacier. *Earth and Planetary Science Letters*, **399**, 10.1016/j.espl.2014.05.001.

Toutin, T. 2002. Three-dimensional topographic mapping with ASTER stereo data in rugged topography. *IEEE Transactions on Geoscience and Remote Sensing*, **40**, 2241–2247.

Ushio, S., Wakabayashi, H. & Nishio, F. 2006. Sea ice variation in Lützow–Holmbukta, Antarctica, during the last fifty years. *Journal of the Japanese Society of Snow and Ice*, **68**, 299–305 [in Japanese with English abstract].

Ushio, S. 2010. Land-fast ice variation in Lützow–Holm Bay, Antarctica, during the past eight decades. *Summaries of JSSI & JSSE Joint Conference on Snow and Ice Research, 2010*, **B3–15**, 209.

Ushio, S. 2012. Sea ice condition in Lützow-Holm Bay, Antarctica, in the austral summer of 2011/12. *Summaries of JSSI & JSSE Joint Conference on Snow and Ice Research, 2012*, **C3–1**, 72.

Whitworth, T., Orsi, A.H., Kim, S.J., Nowlin, W.D. & Locarnini, R.A. 1998. Water masses and mixing near the Antarctic Slope Front. *Antarctic Research Series*, **75**, 1–28.

Wingham, D.J., Wallis, D.W. & Shepherd, A. 2009. Spatial and temporal evolution of Pine Island Glacier thinning, 1995–2006. *Geophysical Research Letters*, **36**, 10.1029/2009GL039126.

Yu, J.Y., Liu, H.X., Jezek, K.C., Warner, R.C. & Wen, J.H. 2010. Analysis of velocity field, mass balance, and basal melt of the Lambert Glacier – Amery Ice Shelf system by incorporating Radarsat SAR interferometry and ICESat laser altimetry measurements. *Journal of Geophysical Research - Solid Earth*, **115**, 10.1029/2010JB007456.